Spatial distortion of vibration modes via magnetic correlations of impurities

F. S. Krasniqi[1,2*], Y. Zhong[1,2,3*], S. W. Epp[1,3,4], L. Foucar[1,2], M. Trigo[5], J. Chen[5], D. A. Reis[5], H. L. Wang[6], J. H. Zhao[6], H. T. Lemke[7†], D. Zhu[7], M. Chollet[7], D. M. Fritz[7], R. Hartmann[8], L. Englert[9‡], L. Strüder[1,8,9,10], I. Schlichting[1,2] and J. Ullrich[1,3§]

[1]*Max Planck Advanced Study Group at CFEL, Notkestr. 85, 22607 Hamburg, Germany.*
[2]*Max Planck Institute for Medical Research, Jahnstr. 29, 69120 Heidelberg, Germany.*
[3]*Max Planck Institute for the Structure and Dynamics of Matter, Luruper Chaussee 149, Bldg. 99 (CFEL), 22761 Hamburg, Germany.*
[4]*Max Planck Institute for Nuclear Physics, Saupfercheckweg 1, 69117 Heidelberg, Germany.*
[5]*Stanford PULSE and SIMES Institutes, SLAC National Accelerator Laboratory, Menlo Park, CA 94025, USA.*
[6]*State Key Laboratory of Superlattices and Microstructures, Institute of Semiconductors, Chinese Academy of Sciences, P.O. Box 912, Beijing 100083, P.R. China.*
[7]*Linac Coherent Light Source, SLAC National Accelerator Laboratory, Menlo Park, CA 94025, USA.*
[8]*PNSensor GmbH, Römerstr. 28, 80803 München, Germany.*
[9]*Max Planck Institute for Extraterrestrial Physics, Giessenbachstrasse 1, 85748 Garching.*
[10]*Max-Planck-Society Semiconductor Laboratory, Otto-Hahn-Ring 6, 81739 München, Germany.*
[‡]*Present address: Institute of Physics, Carl von Ossietzky University Oldenburg, Carl-von-Ossietzky-Strasse 9-11, 26129 Oldenburg, Germany.*
[†]*Present address: SwissFEL, Paul Scherrer Institut, 5232 Villigen PSI, Switzerland.*

*Correspondence to: faton.s.krasniqi@web.de and yinpeng.zhong@mpsd.mpg.de

Content

A) Materials and Methods

The experiment has been performed at the LCLS [1, 2] using 10.363 keV, 50 fs x-ray pulses at a repetition rate of 120 Hz. The x-ray beam was focused to a 0.5×0.5 mm^2 spot in the sample yielding an incident fluence of about 0.6 mJ/cm^2. The x-ray bandwidth $\Delta E/E$ was about 10^{-4}. Time dependent changes in the diffracted intensity around (004) Bragg reflection were measured by a PIPS diode, see Fig. S1. At a variable time relative to the arrival of the x-ray pulses, a *p*-polarized femtosecond laser pump pulse (λ_{las}=800 nm, τ_{FWHM}=50 fs), nearly collinearly with the x-ray beam (clearance of ~0.6 deg), focused down to a 1.0×1.8 mm^2 spot, excites the sample with an absorbed fluence of about 4 mJ/cm^2. Each data point in Figs. 1 and 2 in the manuscript has been averaged over 360 pulses.

The x-ray photon energy E_x=10.363 keV was referenced near to the Ga K-edge (10.367 keV) in order to observe, in addition to x-ray diffraction, the onset of ferromagnetic phase by collecting the fluorescence intensity by a large area, energy and position dispersive, single-electron counting pnCCD detector devices [3].

The experiment has been designed to observe long wavelength longitudinal acoustic phonons which are excited in the $Ga_{0.91}Mn_{0.09}As$ film. To avoid excitation of the substrate, the sample thickness was chosen to be larger than the laser penetration depth ζ. Since laser generated coherent acoustic phonons have a *q*-space distribution which peaks around the inverse of laser penetration depth, q_{peak}~1/ζ , a near infrared beam with λ=800 nm and large penetration depth (ζ≈700 nm) has been used to excite the sample.

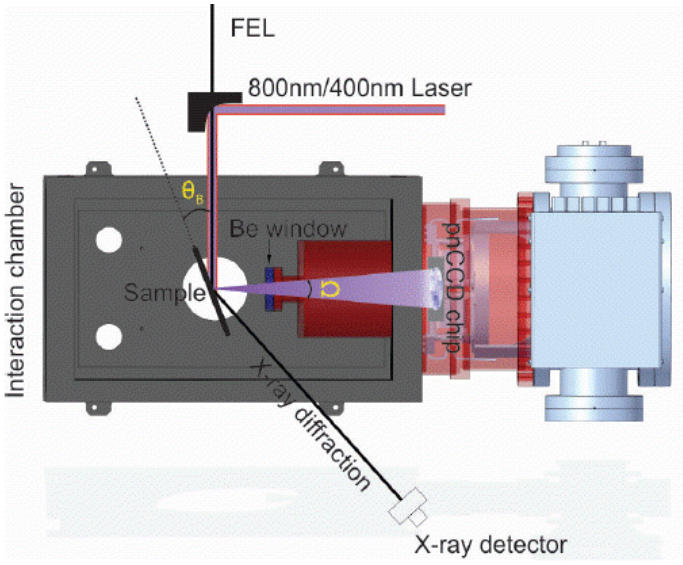

Fig. S1 Scheme of the experimental setup (top view). Time dependent changes in the diffracted intensity around (004) Bragg reflection were measured by a PIPS diode. In addition to x-ray diffraction, we have observed the onset of ferromagnetic phase by collecting the fluorescence intensity by a large area, energy and position dispersive, single-electron counting pnCCD detector devices. In a vacuum chamber with pressure on the order of 10^{-5} mbar, the sample was attached to a cold finger that was in thermal contact with a liquid helium bath.

A 1 μm-thick GaMnAs epitaxial film with a nominal Mn composition of 9%, (001) surface orientation and 1 μm thick $Al_{0.2}Ga_{0.8}As$ buffer layer, was grown by low temperature molecular-beam epitaxy technique [4]. The Mn flux, and hence the nominal Mn doping *x*, including all the possible occupied sites such as the Ga lattice and the interstitial sites, was estimated by measuring the ratio of the beam equivalent pressures of Mn and Ga sources. The sample was then cut into several pieces, and annealed at different temperatures in the air for 1 hour, see Fig. S2. Temperature dependence of the remnant magnetization (M-T) along GaAs [-110] direction (easy axis) were measure by SQUID magnetometer with 2 mT nominal magnetic field. The irregular shape of the magnetization curve at around T=30 K (see also Fig. S3) is due to the change of the preferential magnetization axis at this temperature, an effect which results from the interplay of in-plane biaxial and uniaxial anisotropy fields [5].

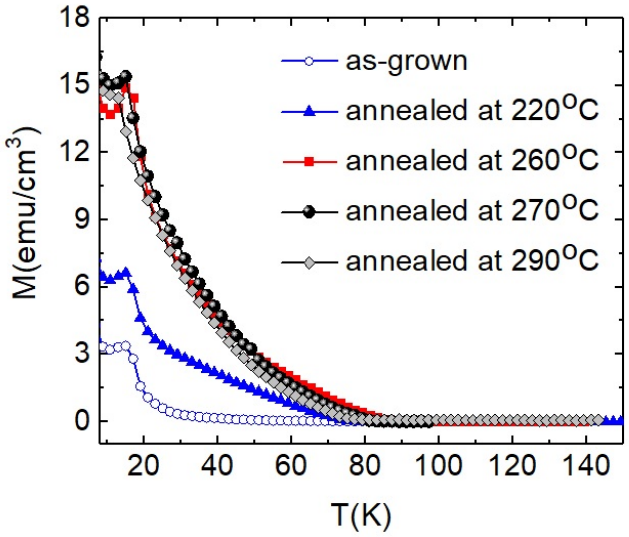

Fig. S2 Temperature dependence of the remnant magnetization of $Ga_{0.91}Mn_{0.09}As$ pieces annealed at different temperatures and measured along [-110] direction using a SQUID magnetometer with 2 mT nominal magnetic field.

Our sample has been annealed in air at 270°C for one hour. As the required annealing time to reduce the compensating defects increases with sample thickness [6], a large fraction of Mn interstitials are not passivated (e.g. by oxidation due to the diffusion at the surface) but will act like a double donors that reduce the total magnetic moment by antiferromagnetic coupling of their spin with the substitutional Mn spin, and likely form pairs with a net magnetic moment close to zero [7]. The partial concentrations of substitutional and interstitials impurities, $x_s \approx 0.055$ and $x_i \approx 0.035$, respectively, have been estimated from the saturation magnetization (~16 emu/cm^3) assuming (*a*) the interstitial atoms form pairs with substitutional Mn atoms, yielding thus to an effective substitutional doping $x_{s,eff} \approx 0.02$, and (b) the magnetic moment per $x_{s,eff}$ is $4\mu_B$. These numbers compare well with those calculated using the TBA (tight binding approximation) approach presented by Jungwirth *et al*. (2005) [8] where, for a nominal doping x=0.09, one finds $x_{s,TBA}$=0.07 and $x_{i,TBA}$=0.02. Although for thick GaMnAs samples (thicker than 500 nm) a realiable measurement of intrinsic semiconducting and

magnetic properties is difficult [6], the onset of ferromagnetic state at $T_c \approx 90$K was observed, which corroborates with our x-ray diffraction data that measure scattering of phonons from spin fluctuations and show a critical behavior around 90 K (Fig. 2, manuscript).

To check the emergence of a superparamagetic-like spin arrangement observed by Sawicki *et al*. (2010) [9], a series of magnetization curves along [-110] have been measured, see Fig. S3. Here, similar to the paper by Sawicki *et al.* [9], the sample has been cooled to T_0=10 K and then, instead of warming the system directly to above T_c, the temperature sweep is interrupted at some intermediate temperatures (T_f =30 K to 150 K) and redirected back to T_0 where the warming is restarted. Our data indicate that the spontaneous magnetization does not depend on the cooling and warming history—the merged curves indicate that superparamagnetic-like portion in our sample, if it exists, might be neglected.

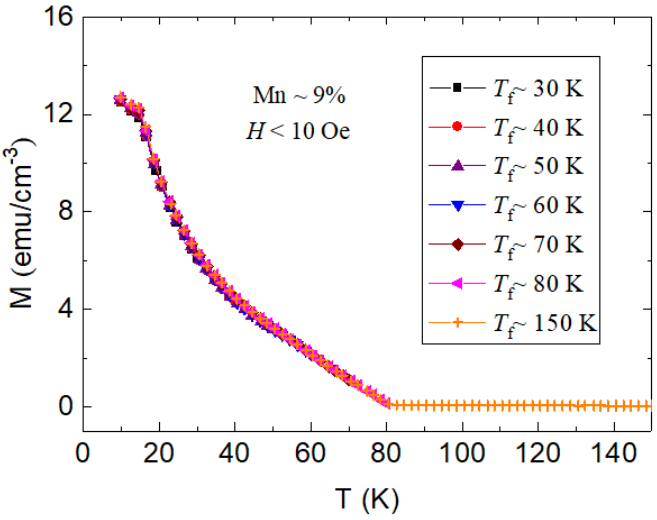

Fig. S3 Temperature dependence of the remnant magnetization of $Ga_{0.91}Mn_{0.09}As$ annealed at 270 °C measured along [-110] to check the reversibility of the ferromagnetic state. The sample has been cooled to T_0=10 K and then, instead of warming the system directly to above T_c, the temperature sweep is interrupted at some intermediate temperatures (T_f=30 K to 150 K) and redirected back to T_0 where the warming is restarted.

B) X-Ray Diffraction as a Tool for Probing Phonon Modes

Time resolved x-ray diffraction is a very powerful tool to directly observe small shifts in the interatomic distance associated with phonons. The sensitivity of x-ray diffraction to coherent lattice dynamics as well as its advantages compared to other methods have been extensively discussed and demonstrated in many experiments in both Bragg and Laue geometries [10-13]. Here we give some brief excerpt which illustrates the idea on how time resolved x-ray diffraction can probe phonon modes of wavelength $\lambda_q = 2\pi / q$.

Coherent acoustic phonons modulate the crystal lattice—they modulate the interplanar spacing by a small amount Δd (on the order of picometers) and thus induce time

dependent strains, see Fig. S4. Since x-ray diffraction is susceptible to shifts in interatomic distances, any new induced periodicity in the lattice, e.g. due to a phonon mode of wavelength $\lambda_q=2\pi/q$, will change the Laue condition to $\Delta\mathbf{K}=\mathbf{G}\pm\mathbf{q}$ and introduce side-bands to the main rocking curve peak at $\Delta\theta_q=q|\mathbf{G}|^{-1}(\tan\theta_B\cos\alpha+\sin\alpha)$, with $\Delta\mathbf{K}$ being the momentum change of x-rays, $\mathbf{G}$ is the reciprocal lattice vector, θ_B the Bragg angle and α =0 is the asymmetry angle for waves propagating along $\mathbf{G}$.

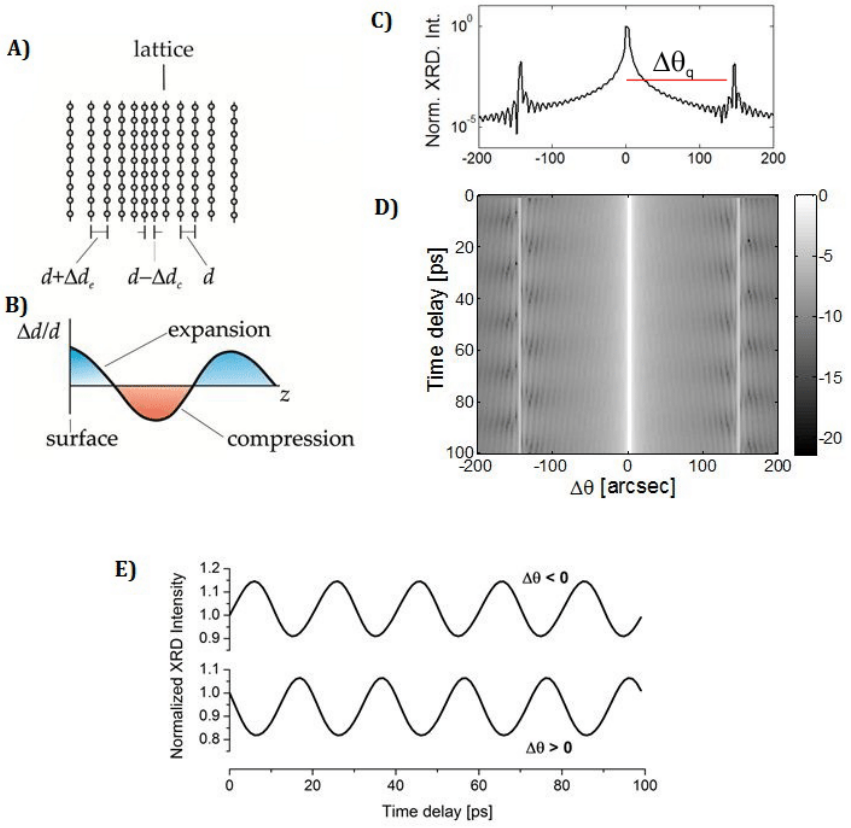

Fig. S4 (**A**) Schematics of a crystal with a single phonon mode. (**B**) Phonons modulate the *d*-spacing between the lattice planes. (**C**) X-ray diffraction from a single coherent acoustic phonon mode $u_q\sin(qz-\omega t)$ leads to the appearance of the side bands at $\Delta\theta_q$. (**D**, **E**) The side band at $\Delta\theta_q$ is related to the phonon wavevector q by the relation $q(\Delta\theta)=\Delta\theta|\mathbf{G}|/\tan(\theta_B)$, and oscillates at the phonon frequency $\omega_q\approx vq$, with v being the speed of sound.

Excitation of the sample with the laser light generates a broad distribution of phonons [10, 14]. Different phonon modes are selected out by measuring the time dependent x ray diffraction at particular position in the rocking curve (i.e. at a particular angle $\Delta\theta_q$ from the Bragg peak), see Fig. S5.

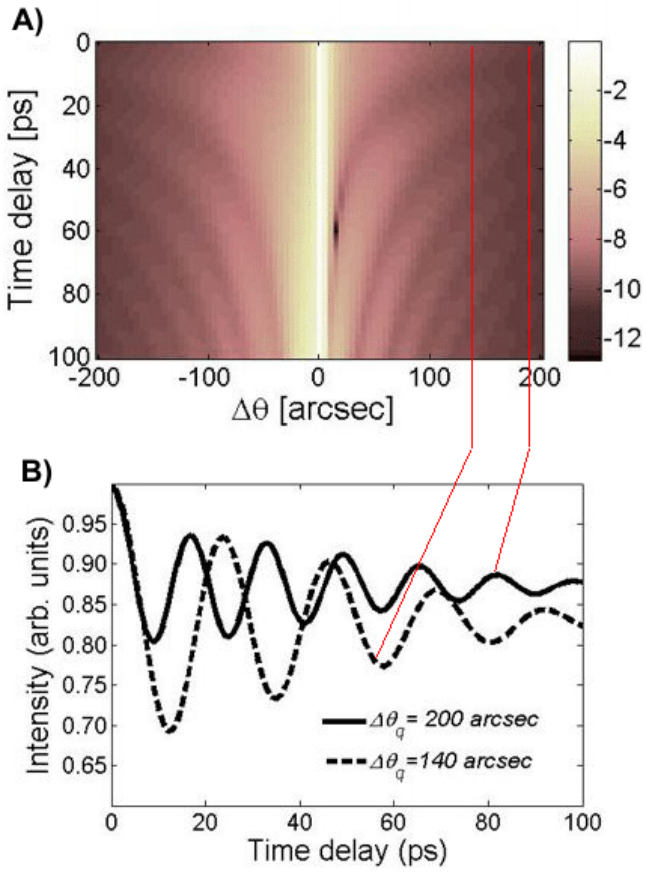

Fig. S5 (**A**) Simulated time dependent x-ray diffraction from a superposition of coherent longitudinal acoustic phonons in GaMnAs. (**B**) Different phonon modes are selected out by measuring the time dependent x-ray diffraction at particular positions $\Delta\theta_q$ in the rocking curve.

C) Spin-Phonon Interaction

In a crystal containing magnetic atoms, spins and lattice vibrations are correlated. This correlation, the so-called spin-phonon interaction, occurs because the displacements of magnetic atoms from their equilibrium positions due to phonons will change the distance between the neighboring spins and, thus, will lead to a change in the exchange interaction [15-18].

The total potential energy of a non-magnetic host crystal with magnetic impurities can be written as a sum of lattice and spin contributions,

$$U_{tot} = U_L + U_S \,. \qquad \text{(S1)}$$

Here U_L is the lattice potential energy. In the harmonic approximation [19],

$$U_L = U_0 + \frac{1}{4}\sum_{m,n} \frac{\partial^2 \Phi(\mathbf{R}_m - \mathbf{R}_n)}{\partial u^2} (\mathbf{u}_m - \mathbf{u}_n)^2 \,, \qquad \text{(S.2)}$$

where $\mathbf{R}_m$ is the average position of atom m, $\mathbf{u}_m$ is the displacement of atom m from its

average position $\mathbf{R}_m$, Φ is the interaction energy per atom-pair and U_0 is the equilibrium potential energy (cohesive energy). In this expression, the indices m and n run over all atoms in the crystal.

To quantify the spin contribution U_S on the lattice potential energy, one can start with the expression of the exchange energy between two magnetic atoms located a positions $\mathbf{r}_i$ and $\mathbf{r}_j$,

$$U_S = -\frac{1}{2}\sum_{i,j} J\left(\mathbf{r}_i - \mathbf{r}_j\right)\left\langle \mathbf{S}_i \mathbf{S}_j \right\rangle , \tag{S3}$$

where $J(\mathbf{r}_i - \mathbf{r}_j)$ is the exchange interaction and $\langle \mathbf{S}_i \mathbf{S}_j \rangle$ is the two-spin correlation function [15-18]. Since the instantaneous position $\mathbf{r}_i(t)$ can be expressed as $\mathbf{r}_i(t)=\mathbf{R}_i+\mathbf{u}_i(t)$, the dynamical variable $\mathbf{u}_i(t)$ will enter the exchange interaction

$$J\left(\mathbf{r}_i - \mathbf{r}_j\right) = J\left(\mathbf{R}_i - \mathbf{R}_j + \mathbf{u}_i(t) - \mathbf{u}_j(t)\right) \tag{S4}$$

which, then, can be written as Taylor series,

$$J\left(\mathbf{r}_i - \mathbf{r}_j\right) = J\left(\mathbf{R}_i - \mathbf{R}_j\right) + \frac{\partial J\left(\mathbf{R}_i - \mathbf{R}_j\right)}{\partial \mathbf{u}}\left(\mathbf{u}_i - \mathbf{u}_j\right) + \frac{1}{2}\frac{\partial^2 J\left(\mathbf{R}_i - \mathbf{R}_j\right)}{\partial u^2}\left(\mathbf{u}_i - \mathbf{u}_j\right)^2 + \cdots \tag{S5}$$

Substituting Eq. (S5) into (S3) we obtain

$$U_S = -\frac{1}{2}\sum_{i,j}\left\langle \mathbf{S}_i \mathbf{S}_j \right\rangle \left[J\left(\mathbf{R}_i - \mathbf{R}_j\right) + \frac{\partial J\left(\mathbf{R}_i - \mathbf{R}_j\right)}{\partial \mathbf{u}}\left(\mathbf{u}_i - \mathbf{u}_j\right) + \frac{1}{2}\frac{\partial^2 J\left(\mathbf{R}_i - \mathbf{R}_j\right)}{\partial u^2}\left(\mathbf{u}_i - \mathbf{u}_j\right)^2 + \cdots \right] . \tag{S6}$$

Using Eqs. (S2) and (S6), the total potential energy of the crystal U_{tot} can be written as

$$U_{tot} = U_0 - \frac{1}{2}\sum_{i,j}\left\langle \mathrm{S}_i \mathrm{S}_j \right\rangle J\left(\mathrm{R}_i - \mathrm{R}_j\right) - \frac{1}{2}\sum_{i,j}\left\langle \mathrm{S}_i \mathrm{S}_j \right\rangle \frac{\partial J\left(\mathrm{R}_i - \mathrm{R}_j\right)}{\partial \mathrm{u}}\left(\mathrm{u}_i - \mathrm{u}_j\right) + \frac{1}{4}\left\{ \sum_{m,n}\frac{\partial^2 \Phi\left(\mathrm{R}_m - \mathrm{R}_n\right)}{\partial u^2}\left(\mathrm{u}_m - \mathrm{u}_n\right)^2 - \sum_{i,j}\left\langle \mathrm{S}_i \mathrm{S}_j \right\rangle \frac{\partial^2 J\left(\mathrm{R}_i - \mathrm{R}_j\right)}{\partial u^2}\left(\mathrm{u}_i - \mathrm{u}_j\right)^2 \right\} . \tag{S7}$$

In this equation,

- the zeroth order term in $(\mathbf{u}_i\text{-}\mathbf{u}_j)$ determines the ground state spin configuration,
- the linear term in $(\mathbf{u}_i\text{-}\mathbf{u}_j)$ provides the magnetic force for the lattice distortion (magnetostriction), and
- the term quadratic in $(\mathbf{u}_i\text{-}\mathbf{u}_j)$ affects the phonon dispersion.

In Eq. (S7) the second derivative of the potential energy Φ with respect to the displacement u gives us the elastic spring constant

$$k_{mn} = \frac{\partial^2 \Phi(\mathbf{R}_m - \mathbf{R}_n)}{\partial u^2} \quad . \tag{S8}$$

Similarly, we can define a magnetic spring constant Δk_{ij}, which represents the contribution of the exchange interaction on k_{ij}, as

$$\Delta k_{ij} = \frac{\partial^2 J}{\partial u^2} \langle \mathbf{S}_i \mathbf{S}_j \rangle \quad . \tag{S9}$$

With these definitions, the term quadratic in displacement can be rewritten as

$$\frac{1}{4} \left\{ \sum_{m,n} k_{mn} (\mathbf{u}_m - \mathbf{u}_n)^2 - \sum_{i,j} \Delta k_{ij} (\mathbf{u}_i - \mathbf{u}_j)^2 \right\} \tag{S10}$$

D) Space Discretization of Elastic Continuum Equation

Our time dependent x-ray diffraction data demonstrate that at room temperature the probed acoustic modes can be well described by elastic waves conform to the Thomsen equation [20],

$$\frac{\partial^2 u}{\partial t^2} = v^2 \frac{\partial^2 u}{\partial z^2} + \frac{R(z)}{\rho} \quad , \tag{S11}$$

where u is the displacement, v is the longitudinal speed of sound, ρ is the mass density and $R(z)$ is a source term which depends on the excitation energy and wavelength. Spatial distortion of vibrational modes indicates inhomogenities in the medium. In this case, the atomic details of the medium need to be considered. To include these details in our modelling, we start with the equation that describes the propagation of elastic waves through an inhomogeneous medium,

$$\rho(z) \frac{\partial^2 u}{\partial t^2} = \frac{\partial}{\partial z} \left(G(z) \frac{\partial u}{\partial z} \right) + R(z) \quad , \tag{S12}$$

where $G(z)$ is the elastic modulus. By using the forward discretization scheme with a step size Δz equal to the lattice constant a,

$$\frac{\partial}{\partial z} \left(G(z) \frac{\partial u}{\partial z} \right) \approx k_{j+1} \frac{(u_{j+1} - u_j)}{a^3} - k_j \frac{(u_j - u_{j-1})}{a^3} \quad , \tag{S13}$$

with $k_j = aG_j$, we obtain

$$m_j \frac{d^2 u_j}{dt^2} = k_{j+1}(u_{j+1} - u_j) + k_j (u_{j-1} - u_j) + F(z_j) \quad , \tag{S14}$$

where $F = a^3 R$. Equation (S14) represents a linear chain composed of N particles, each with a mass m_j, see Fig. S6. Modelling approaches based on the linear chain of masses have been successfully used in the past to understand the excitation response of the sample and to visualize the dynamics of the lattice [21,22].

Equation (S14) describes the motion of a particle in a chain which stores the potential energy

$$U = U_0 + \frac{1}{2}\sum_j k_j \left(u_{j+1} - u_j\right)^2 + \sum_j F_j u_j \quad . \tag{S15}$$

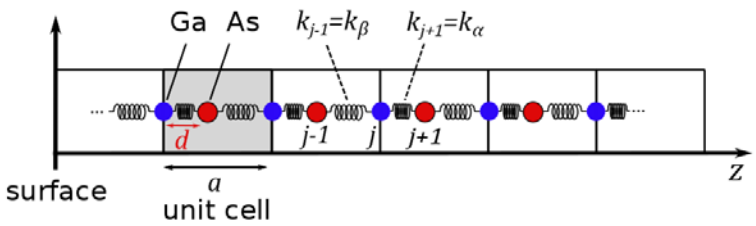

Fig. S6 Schematic illustration of a linear chain concept which results from the spatial discretization of Eq. (S12). The unit cell contains both basis atoms, Ga atom at the origin and As atom at $d=a/4$ (in a 3D lattice, $a/4$ is the fractional coordinate of the As atom along the [001] direction). $k_{j+1}=k_\alpha$ and $k_{j-1}=k_\beta$ are the effective force constants between the layers (j, j+1) and (j, j-1).

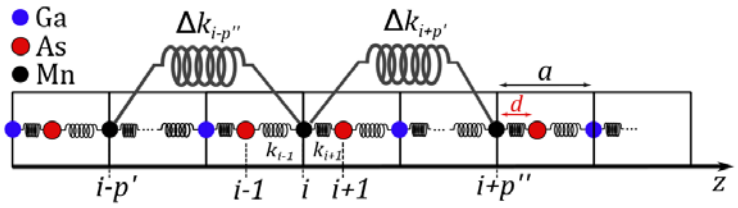

Fig. S7 Schematic illustration of a linear chain containing magnetic impurities. Spin-phonon interaction contributes on the vibrations of the chain by adding a spring constants $\Delta k_i \approx -J''(u)\langle \mathbf{S}_0\mathbf{S}_1\rangle$ which connect the neighboring impurity atoms i+p' and i-p'' with the central atom i.

If the chain contains magnetic impurities (see Fig. S7) then, according to Eq. (S7), the potential energy becomes

$$\begin{aligned} U_S &= U_0 - \sum_i J\left(z_i - z_{i+1}\right)\left\langle \mathbf{S}_i\mathbf{S}_{i+1}\right\rangle \\ &- \sum_i \left\langle \mathbf{S}_i\mathbf{S}_{i+1}\right\rangle \frac{\partial J}{\partial u}\left(u_i - u_{i+1}\right) + \sum_j F_j u_j \\ &+ \frac{1}{2}\left\{\sum_j k_j\left(u_j - u_{j+1}\right)^2 - \sum_i \Delta k_i \left(u_i - u_{i+1}\right)^2\right\} \end{aligned} \quad . \tag{S16}$$

In this equation, the index j runs through all atoms whereas index i through impurity atoms only.

The equation of motion for an atom m_n is

$$\begin{aligned} m_n \frac{d^2 u_n}{dt^2} &= k_{n+1}\left(u_{n+1} - u_n\right) + k_{n-1}\left(u_{n-1} - u_n\right) + F_n \\ &+ r\Delta k_{mag}\left(u_{n+p'} - u_n\right) + r\Delta k_{mag}\left(u_{n-p''} - u_n\right) + r f_n \end{aligned} \quad , \tag{S17}$$

with m_n being the mass of an Ga, As, or Mn atom (depending on the layer, cf. Fig. S6 and S7) , k_{n+1} and k_{n-1} are the effective force constants between the layers (n, n +1) and (n, n-

1), respectively, and $\Delta k_{mag} \approx -J''(u)\langle \mathbf{S}_0\mathbf{S}_1\rangle$. Indices *p'* and *p''* stand for the nearest neighbor impurity atoms, and $f_i \approx \langle S^2\rangle dJ/du$. For a host atom $r = 0$, whereas for an impurity atom $r = 1$.

The motion of all atoms in the chain, including both hosts and impurities, can be cast into a matrix form

$$[\mathbf{M}]\cdot\left[\frac{d^2\mathbf{U}}{dt^2}\right] = -[\mathbf{K}]\cdot[\mathbf{U}] + [\mathbf{F}] \tag{S18}$$

where, [**M**] is N×N diagonal matrix. For an impurity atom at the site $i=3$, for example, we can write

$$[\mathbf{M}] = \begin{bmatrix} M_{Ga} & 0 & 0 & 0 & 0 & \cdots & 0 & 0 \\ 0 & M_{As} & 0 & 0 & 0 & \cdots & 0 & 0 \\ 0 & 0 & M_{imp} & 0 & 0 & \cdots & 0 & 0 \\ 0 & 0 & 0 & M_{As} & 0 & \cdots & 0 & 0 \\ 0 & 0 & 0 & 0 & M_{Ga} & \cdots & 0 & 0 \\ \vdots & \vdots & \vdots & \vdots & \vdots & \ddots & \vdots & \vdots \\ 0 & 0 & 0 & 0 & 0 & \cdots & M_{Ga} & 0 \\ 0 & 0 & 0 & 0 & 0 & \cdots & 0 & M_{As} \end{bmatrix}$$

[**K**] is $N \times N$ force constant matrix. Its elements are:

$$\begin{aligned}
\mathbf{K}_{i-1,i-1} &= k_\alpha + k_\beta^* \\
\mathbf{K}_{i-1,i} &= -k_\beta^* \\
\mathbf{K}_{i,i-1} &= -k_\beta^* \\
\mathbf{K}_{i,i} &= k_\alpha^* + k_\beta^* + 2r\Delta k_{mag} \\
\mathbf{K}_{i,i+1} &= -k_\alpha^* \\
\mathbf{K}_{i+1,i} &= -k_\alpha^* \\
\mathbf{K}_{i+1,i+1} &= k_\beta + k_\alpha^* \\
\mathbf{K}_{i,i+p} &= -r\Delta k_{mag} \\
\mathbf{K}_{i,i-p} &= -r\Delta k_{mag} \\
\mathbf{K}_{i+p,i} &= -r\Delta k_{mag} \\
\mathbf{K}_{i-p,i} &= -r\Delta k_{mag}
\end{aligned} \quad .$$

where, k^*_α and k^*_β are force constants for the impurity atoms whereas k_α and k_β for the host atoms. Other elements in the [**K**] matrix are zero.

Interstitial atoms Mn_I are assumed to form pairs with substitutional atoms Mn_{Ga}. Such a Mn_I-Mn_{Ga} pair is assumed to have zero magnetic moment [7,8] and is represented by a pseudoatom with a mass $2m_{Mn}$, where m_{Mn} is the mass of a Mn atom, see Fig. S8.

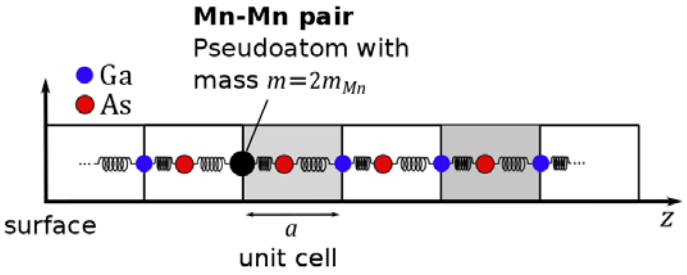

Fig. S8 Inclusion of interstitials. Mn substitutional and Mn interstitial atoms form a pair with zero magnetic moment, and are represented by a pseudoatom with a mass $2m_{Mn}$, where m_{Mn} is the mass of Mn atom.

[**U**] is $N\times1$ displacement matrix. Its elements are displacements of atoms in the chain: $[\mathbf{U}]=[U_1,U_2,U_3,\cdots,U_N]$.

[**F**] is $N\times1$ force matrix. Its elements are: $F_{i1}=-(rf_i+F_i)$.

By using the transformation [21]

$$[\mathbf{u}]=[\mathbf{U}]-[\mathbf{K}]^{-1}[\mathbf{F}], \tag{S19}$$

the inhomogeneous matrix equation (S18) is transformed into a homogeneous one

$$[\mathbf{M}]\cdot\left[\frac{d^2\mathbf{u}}{dt^2}\right]=-[\mathbf{K}]\cdot[\mathbf{u}] \tag{S20}$$

.

Following Barker and Sievers [23], by assuming

$$[\mathbf{u}]=[\mathbf{A}]\exp(i\omega t), \tag{S21}$$

with [**A**] being the amplitude (normal mode) matrix, Equation (S20) can be transformed into an eigenvalue problem

$$\omega^2[\mathbf{M}]\cdot[\mathbf{A}]=-[\mathbf{K}]\cdot[\mathbf{A}] \tag{S22}$$

Solution of this equation gives N eigenvalues and N eigenvectors A_Q. Here Q is a parameter which describes the spatial periodicity.

E) Effect of doping level on the quasilocalization of vibrational modes

Quasilocalization of long wavelength vibration modes depends strongly on the magnetic force constant $\Delta k_{mag}=-(d^2J/du^2)\langle\mathbf{S}_0\mathbf{S}_1\rangle$. The width of vibrational modes Δq increases monotonically with Δk_{mag} but not with the doping level x, see Fig. S9. A minimum doping level which affects considerably the periodicity of the vibration modes is about 0.5%. In this case, all modes with wavevector smaller than 0.003 π/a lose their spatial periodicity. The dependence of quasilocalization of vibrational modes with doping level

above $x \approx 5\%$ can be explained in terms of the magnetic force $F_{mag} = \Delta k_{mag} (u_i - u_j)$, where u_i and u_j are displacements of two neighboring magnetic atoms. For a constant Δk_{mag}, the effect of magnetic force on the quasilocalization of vibrational modes is largest when $(u_i - u_j)$ is large. With increasing doping level, the distance between magnetic atoms decreases; This leads to a small $(u_i - u_j)$ at large wavelengths since the number of impurity atoms populating the same crest (or the same trough) increases.

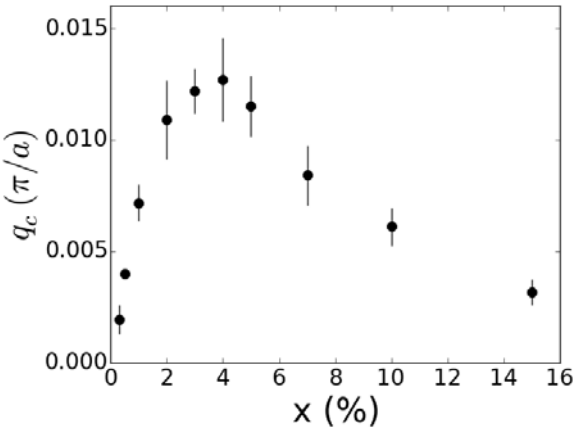

Fig. S9 The effect of doping level on the quasilocalization of vibrational modes. q_c represents the wavevector below which the spatial periodicity of vibrational modes is destroyed (i.e. modes with $q<q_c$ cannot sample the spatial periodicity of the lattice) and x the concentration of substitutional impurities. The wavevector q_c has been calculated using the approach described in Section D (Eqs. 18-22) with concentration of interstitials x_i=3.5%, no antisites, Δk_{mag}=-26 meV/Å^2 and was averaged over 20 random configurations of impurities.

F) The effect of various interactions in the quasilocalization of vibrational modes

Impurities typically perturb the energetics of the crystal by producing an alternation in the kinetic energy due to the mass difference relative to the host atom and by modifying the force constants around the impurity atom.

When impurity atoms are less massive than the host atoms (which is the case of Mn in GaAs) or, when they are coupled to neighboring atoms more strongly than host atom do, localized vibrational modes will appear [23]. These modes are characterized by large vibrational amplitudes at the impurities and its immediate neighbors while the rest of atoms is not displaced, see Fig. S10 (a). These modes, however, have frequencies which lie outside the acoustic branch of the host crystal (they lie in the gap between the acoustic and optical branch, or in the gap between two optical branches) and do not affect phonon dispersion at low frequencies.

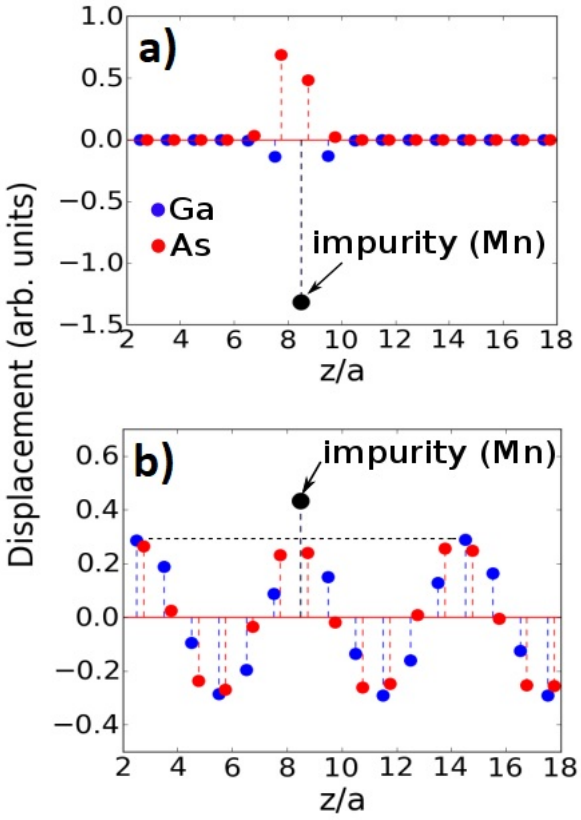

Fig. S10 Eigenvectors of (**a**) localized and (**b**) resonant modes in a GaAs chain containing Mn impurities.

When Mn impurity atoms are coupled weakly to their neighbors than the host atoms do, resonant modes with frequencies within the acoustic branch of the host crystal will occur [23,24]. Here, all atoms vibrate in a sinusoidal patterns but with extra amplitude at the impurity atom, see Fig. S10 (b). They are activated only when the reduction of force constant is large, typically more than 50% and will manifest themeselves as broad peaks in the density of states (i. e. will modify the dispersion relation locally). Even when reduction of force constants is very large $\gamma=(k-k')/k=90\%$, with k and k' being the nearest-neighbor force constants for the host and impurity atoms, respectively, resonant modes will have frequencies around $\nu_{res}\sim(6k'/M_{impurity})^{1/2}/2\pi \approx 0.18$ THz which is more than four times higher than frequencies involved in our work. Being, however, able to measure well defined phonon modes with a linear dispersion at the room temperature, where the impurities are not correlated but are still in the host lattice, implies that resonant modes do not affect phonon dispersion at small wave vectors. Weakly bound impurities do not affect long wavelength modes because the impurity is "*carried over*" by the two neighboring host atoms to move in a sinusoidal envelope of the host vibrational modes. This balance is disrupted when an impulse is exerted upon by another impurity, for example, when impurities are correlated. In our case, even though the magnetic force constant Δk_{mag} is only few percent of the spring constant connecting the impurity with its nearest neighbors, it is still enough to introduce a phase shift on the displacement at the impurity atom. In contrast to resonant modes where impurity atoms gain extra displacements (and thus, force constants need to be reduced considerably to allow that),

magnetic correlations affect the vibrational modes by introducing a phase shift at the impurity atoms.

The effect of various interactions in the quasilocalization of vibrational modes is shown in Fig. S11. Here we plot the wavevector q_c below which the spatial periodicity of vibrational modes is destroyed (i.e. modes with $q<q_c$ cannot sample the spatial periodicity of the lattice) when various interactions are taken into account or are omitted. Here, we assume $x_{s,eff}$=2%, x_i=3.5% and x_a=3.5% antisites (since the formation energies of Mn interstitials and As antisites have roughly the same value [25], we have assumed $x_i=x_a$). Small q modes are affected considerably only when reduction of force constants is very large. In this case the impurity atoms are loosely bound so they can act independently of their neighbors. When reduction of force constants is small (<50%) the impurity atoms are forced to follow the displacement envelope of their nearest neighbors.

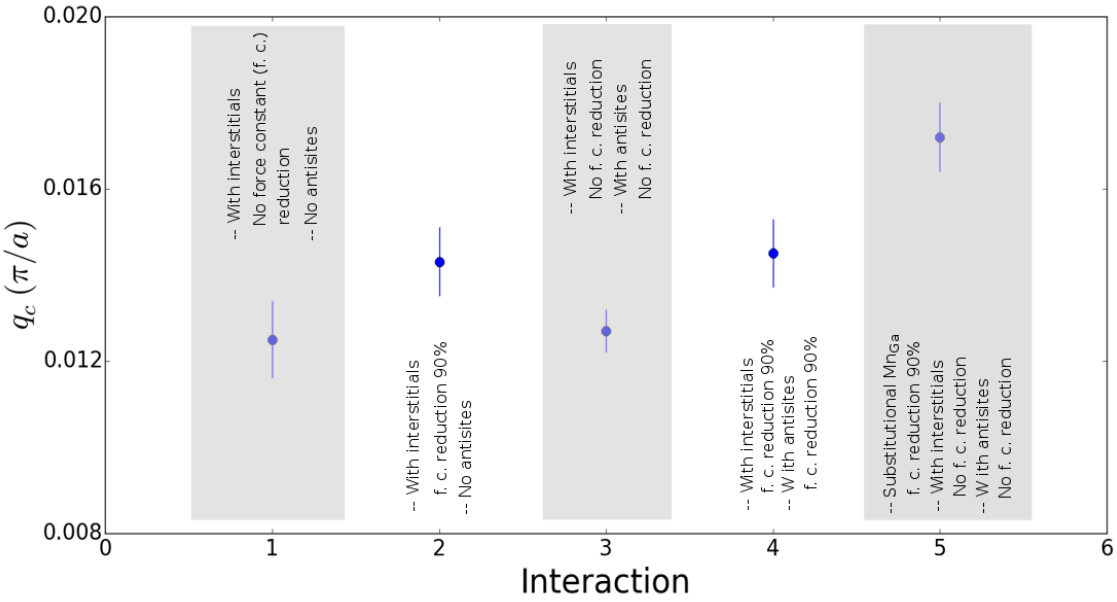

Fig. S11 The effect of various interactions in the quasilocalization of vibrational modes. q_c represents the wavevector below which the spatial periodicity of vibrational modes is destroyed (i. e. modes with $q<q_c$ cannot sample the spatial periodicity of the lattice). *Column 1*: interstitials are taken into account, force constants on each side of interstitials have not been reduced, antisites were not taken into account. *Column 2*: interstitials were taken into account, force constants on each side of interstitials have been reduced by 90%, antisites were not taken into account. *Column 3*: interstitials were taken into account without reducing their force constants, antisites were taken into account (without reducing force constants on each side of antisites). *Column 4*: interstitials were taken into account, force constants on each side of interstitials have been reduced by 90%, antisites were taken into account (force constants on each side of antisites were reduced by 90%). *Column 5*: force constants on each side of substitutional atoms have been reduced by 90%, interstitials were taken into account, force constants on each side of interstitials have not been reduced, antisites were taken into account (without reducing force constants on each side of antisites). The wavevector q_c has been calculated using the approach described in Section D (Eqs. 18-22), Δk_{mag}=-26 meV/Å^2 and was averaged over 20 random configurations of defects.

G) References

[1] M. Chollet *et al*., J. Synchrotron Rad. **22**, 503 (2015).
[2] W. E. White *et al*., J. Synchrotron Rad. **22**, 472 (2015).
[3] L. Strüder *et al*., Nucl. Instrum. Methods A **614**, 483 (2010).
[4] L. Chen *et al*., Appl. Phys. Lett. **95**, 182505 (2009).
[5] K. -Y. Wang *et al*., Phys. Rev. Lett. **95**, 217204 (2005).
[6] P. Nemec *et al*., Nature Communications **4**, 1422 (2013).
[7] J. Blinowski and P. Kacman, Phys. Rev. B **67**, 121204 (2003).
[8] T. Jungwirth *et al*., Phys. Rev. B **72**, 165204 (2005).
[9] M. Sawicki *et al*., Nature Physics **6**, 22 (2010).
[10] A. M. Lindenberg *et al*., Phys. Rev. Lett. **84**, 111 (2000).
[11] D. A. Reis *et al*., Phys. Rev. Lett. **86**, 3072 (2001).
[12] F. S. Krasniqi *et al*., Phys. Rev. B **78**, 174302 (2008).
[13] M. F. DeCamp *et al*., J. Synchrotron Radiat. **12**, 177 (2005).
[14] P. Ruello and V. E. Gusev, Ultrasonics **56**, 21 (2015).
[15] W. Baltensperger and J.S. Helman, Helv. Phys. Acta **41**, 668 (1968).
[16] K. Wakamura, Solid State Communications **71**, 1033 (1989).
[17] E. Granado *et al*., Phys. Rev. B **60**, 11879 (1999).
[18] Wang *et al*., Phys. Rev. B **77**, 134113 (2008).
[19] N. W. Ashcroft and N. D. Mermin, *Solid State Physics*, Harcourt College Publishers (1976).
[20] C. Thomsen *et al*., Phys. Rev. B **34**, 4129 (1986).
[21] M. Herzog *et al*., Appl. Phys. A **106**, 489 (2012).
[22] J. Li *et al*., Phys. Rev. B **80**, 014304 (2009).
[23] A. S. Barker and A. J. Sievers, Rev. Mod. Phys. **47**, S1 (1975).
[24] A. J. Sievers and S. Takeno, Phys. Rev. **140**, A1030 (1965).
[25] Mašek *et al*., Phys. Rev. B **67**, 153203 (2003).